# PCCP

Accepted Manuscript

ROYAL SOCIETY OF CHEMISTRY

www.rsc.org/pccp

# Framework structured $Na_4Mn_4Ti_5O_{18}$ as electrode for Na-ion storage hybrid devices

**M. Jayakumar[a‡], K. Hemalatha[a,b‡], K. Ramesha[a,b] and A. S. Prakash[a,b]***

[a]CSIR Central Electrochemical Research Institute-Chennai Centre, CSIR-Madras Complex, Taramani, Chennai-600 113, India. CSIR−Network Institutes of Solar Energy (CSIR−NISE)

[b]Academy of Scientific and Innovative Research (AcSIR), CSIR Central Electrochemical Research Institute-Chennai Centre, CSIR-Madras Complex, Taramani, Chennai-600 113, India
* Corresponding Author
‡ These authors contributed equally to this work

## ABSTRACT

Framework structured $Na_4Mn_4Ti_5O_{18}$ possessing S-shaped tunnels for sodium intercalation is reported here as electrode for hybrid sodium ion batteries. Galvanostatic cycling of $Na_4Mn_4Ti_5O_{18}$ vs. Na in the voltage region 1.5 V to 3.95 V exhibits a capacity of 102 mAh/g at 0.1C rate corresponding to a specific capacitance of 149 F/g with a capacity retention of 90% over 50 cycles. The electrochemical analysis using CV measurements revealed the charge storage involving intercalation and pseudocapacitance. For instance, total charge storage of 345 C/g is observed at 0.01mv/s, which is attributed to 63% intercalation and 37% capacitance. $Na_4Mn_4Ti_5O_{18}$ was also studied for sodium ion storage in aqueous medium. It delivered a capacity of 36 mAh/g (144 F/g) in the voltage window of 0 – 0.8 V.

## INTRODUCTION

In the last few decades, lithium ion batteries have emerged as leaders in catering the energy needs of portable electronic devices and electric vehicles due to various advantages they offer.[1] While lithium ion batteries are expected to remain unrivaled in near future for these applications, its limited availability and higher cost necessitates one to look for other suitable alternatives beyond lithium ion batteries. One such energy storage option is sodium ion based energy storage devices.[2] Large and diverse natural availability of sodium, lower cost, safety and electrochemical insertion/extraction behavior similar to lithium makes sodium as an attractive choice for the application.[3-5] In particular, applications such as electrical grid storage where energy density and footprint requirements are less stringent, sodium ion devices are more relevant. These factors have revived the interest in sodium ion based batteries.[2-6] In addition to sodium ion batteries that largely employ air and moisture sensitive materials and electrolytes, electrode materials that are stable in ambient conditions would offer exciting opportunities in aqueous rechargeable batteries[7,8] with regard to safety and cost.

On the other hand, there is a growing interest in hybrid devices that combine intercalation with other energy storage mechanisms such as capacitance.[9-12] Generally in such hybrid devices, the diffusion non-controlled capacitance occurs near the surface while diffusion controlled intercalation occurs through the bulk. For instance using ordered mesoporous $\alpha$-$MoO_3$ as model system Bruce Dunn group reported the significance of high surface materials for such surface reaction driven enhanced energy storage.[10] They demonstrated that pseudocapacitive charge storage in such materials is not only limited to surface redox but can also proceed via intercalation pseudocapacitance into the van der Waal gaps.[10] In a similar approach for Na-ion batteries, Senthilkumar *et al.* reported certain framework compounds of the type $NaMPO_4$ (M=Ni, Co, Mn) that exhibit both intercalation and capacitance based charge storage.[13]

Recently Guo *et al.*[14] reported a tunnel-type $Na_{0.61}Ti_{0.48}Mn_{0.52}O_2$ which is similar in composition and structure to the one reported in the present manuscript. They reported a capacity of 86 mAh/g. However, the origin of such capacity was not fully understood. This necessitates a thorough study on the Na-ion charge storage mechanism of such framework compounds. With this background we choose to study isostructural and stoichiometric $Na_4Mn_4Ti_5O_{18}$, previously reported[15], to understand the charge storage mechanism in such framework compounds. Here we report a detailed study on the electrochemical charge storage in framework structured $Na_4Mn_4Ti_5O_{18}$ in non-aqueous and aqueous media.

## EXPERIMENTAL SECTION

### Synthesis

$Na_4Mn_4Ti_5O_{18}$ was prepared by solid state route in two steps. In the first step, starting materials, $Na_2CO_3$, $Mn_2O_3$ and $TiO_2$ corresponding to molar ratio of 2:2:5 were thoroughly mixed by hand grinding using mortar and pestle. The homogeneously mixed precursors were then calcined in air at 1100°C for 3 h followed with regrinding and reheating at 1000 °C for 3 h. The furnace was naturally cooled till 300°C and the sample was quenched to room temperature. The sample was ground and stored for further studies. Stability of sample in air was examined by exposing sample to atmospheric air for several days (15 days). Similarly, moisture stability was studied by treating the sample with water for several hours (48 h) followed by oven drying at 80°C.

### Material characterization

Powder X-ray diffraction of the synthesized sample was recorded using BRUKER D8 Advance Da Vince diffractometer using CuK$\alpha$ ($\lambda$= 1.5418 Å). The crystallographic parameters were determined by Reitveld method[16] using Fullprof Suite[17] program. Scanning electron microscopy was performed using TESCAN VEGA 3SBH attached with EDS. X-ray photoelectron spectroscopy (XPS) measurements were made with Omicron ESCA Probe spectrometer with monochromatized Al $K_\alpha$ X-rays (1486.6 eV) under ultra high vacuum. Atomic absorption spectrometry (AAS) analysis was carried using Varian Model SPECTRAA 220 Spectrophotometer. Thermogravimetric analysis was carried out using Netzsch STA449F3 TG/DSC Analyzer.

### Electrochemical studies

Electrochemical tests using organic electrolytes were carried out in Swagelok type cells assembled in an argon filled glove box. Half cells were assembled with 85%

compound and 15% SP carbon acting as the cathode and sodium metal as counter anode with an active mass loading of about 2 mg. The electrolyte solution was 1 mol/L $NaPF_6$ dissolved in a mixture of 1:1 volume percent of EC-DMC and glass fiber filter (Whatman) was used as a separator. The cell thus fabricated was cycled galvanostatically in the voltage range 1.5 - 3.95 V at different cycle rates. Typical galvanostatic cycling at C/10 rate corresponds to a current density of 12.8 mA/g. Electrochemical performance in aqueous electrolyte was studied in three electrode cell using glassy carbon coated with $Na_4Mn_4Ti_5O_{18}$ as working, platinum as counter and Ag/AgCl as reference electrodes. The electrodes were prepared by coating the slurry composed of 80% active material, 15% SP carbon and 5% Nafion binder and then dried at 80 ˚C for 10h. The aqueous solution of 1 mol/L $Na_2SO_4$ is used as Na-conducting electrolyte medium. Cyclic voltammetry experiments were carried out with IR compensation which is predetermined using impedance measurement. All electrochemical experiments were performed at ambient temperatures (303 K).

## RESULTS AND DISCUSSION

### Material characterization

The powder X-ray diffraction (XRD) pattern of as prepared $Na_4Mn_4Ti_5O_{18}$ and the Rietveld fit are shown in Figure 1. All the Bragg diffraction lines are fitted to the model system, $Na_4Mn_4Ti_5O_{18}$ (Orthorhombic, Space group: *pbam*, JCPDS 01-076-0785). The refined structural parameters are shown in Table 1. In $Na_4Mn_4Ti_5O_{18,}$ $Mn^{3+}$ has two different coordinations, some of $Mn^{3+}$and $Ti^{4+}$ are in octahedral coordination while the remaining $Mn^{3+}$ are in square pyramid coordination.[15] The octahedra, joined by extensive edge and corner sharing, are linked together by the five-coordinated $Mn^{3+}$ to leave a series of pentagonal and S-shaped tunnels for the sodium ions. The structure is shown in Figure 2. These tunnels are similar to those found in $Na_{0.44}MnO_2$ of which, the S-shaped one is much larger and contains sites for four sodium ions, only half of which are filled. This tunnel structure offers excellent pathway for sodium ion shuttling thus making this compound a potential candidate for sodium ion storage.

SEM images of pristine $Na_4Mn_4Ti_5O_{18}$ and water treated $Na_4Mn_4Ti_5O_{18}$ are shown in Figure 3(a) & (b), their respective EDS patterns are given in (c) & (d).The micrograph indicated well defined long particles in both the samples. EDS analysis indicated the composition of Na, Mn and Ti in pristine sample is proportionate to its theoretical value. These values were corroborated by AAS analysis also. The composition as deduced from AAS is close to the nominal composition of the phase (to be precise, $Na_{3.9}Mn_4Ti_5O_{18}$). The little decrease in sodium content may be attributed to the evaporation of sodium at high temperatures and longer heating durations. EDS of water treated sample indicated lower sodium content in the sample, to be exact the composition corresponding to the formula $Na_xMn_4Ti_5O_{18}$ (X is 2.8-3.2 mole). The partial de-sodiation on water treatment is discussed in later section under aqueous Na-ion storage application.

X-ray photoelectron spectroscopy is used to ascertain the chemical and electronic state of elements in a compound. This information is vital to establish the fate of metal ions in a battery cathode to evolve a suitable electrochemical reaction mechanism during charging – discharging i.e. desodiation – sodiation process and further to understand the performance of the material. Full survey spectrum of $Na_4Mn_4Ti_5O_{18}$ is shown in Figure 4(a). It is composed of strong representative peaks of Na, Mn, Ti, O and C at 1071, 642, 459, 530 and 285 eV, respectively. It is evident from Figure 4(a) that the oxidation states of manganese and titanium are +3 and +4, respectively in the pristine compound.

Adventitious C 1s was observed at 284.7 eV and all binding energies could be referenced to this value. Deconvoluted C 1s spectrum is composed of three peaks as shown in Figure 4(b). The sharp and large peak observed at 284.7 eV corresponds to adventitious carbon[18]. The peaks at 285.7 eV and 289.0 eV could be attributed to defect containing carbon and carboxyl (–C=O) carbons, respectively.[18] The Mn($2p_{3/2},_{1/2}$) peaks are observed at 641.9 and 653.8 eV. The peaks are broad and are deconvoluted into three peaks of $2p_{1/2}$ at 640.8, 641.9 and 643.0 eV (Figure 4(c)) which are attributed to $Mn^{3+}$ in different environments.[19] O 1s spectrum is shown in Figure 4(d). It is composed of three individual peaks at 529.6, 531.0 and 532.6 eV. The first peak at 529.6 eV corresponds to $O_2^{2-}$ anions in the crystal lattice.[20] The peak at 531.0 eV may be due to weakly adsorbed surface species and also due to lattice oxygen with coordination defiency.[20] The weak peak at 532.6 eV is due to surface adsorbed species.[20] As shown in Figure 4(e), titanium 2p has two binding energy peaks at 642.4 and 654.2 eV corresponding to $2p_{3/2}$ and $2p_{1/2,}$

respectively. The binding energy of Na 1s was observed at 1071.7 eV as seen in Figure 4(f).

## Electrochemical studies of $Na_4Mn_4Ti_5O_{18}$ in organic electrolyte

Cyclic voltammetry is a powerful tool to understand the mechanism and kinetics of an electrochemical reaction. Cyclic voltammogram of $Na_4Mn_4Ti_5O_{18}$ vs Na cell is shown in Figure 5. The CV of first cycle is slenderly different from consecutive cycles indicating likely structural evolution during first cycle. Although the observed redox peaks are broad and resolved, there exist two prominent redox couples observed at around 1.9 V/2.6 V (a/a') and 3.05 V/3.44 V (b/b'). These observed peaks are attributed to $Mn^{2+}/Mn^{3+}$ and $Mn^{3+}/Mn^{4+}$ redox couples. $Ti^{4+}/Ti^{3+}$ redox is active only at voltages less than 0.75 V as reported for Na intercalation in nanocrystalline $TiO_2$.[21] As the pristine compound contains $Mn^{3+}$, only one peak corresponding to $Mn^{3+}/Mn^{4+}$ was observed during first charging and two redox couples corresponding to above reaction were observed in all subsequent cycles. Additionally, there were one set of less prominent peaks at 2.16 /1.86 V (c/c') and its intensity was reduced after initial few cycles. These peaks can be attributed to minor structural rearrangement of the lattice during initial cycles.

Galvanostatic charge - discharge experiments on $Na_4Mn_4Ti_5O_{18}$ were performed at C/10 rate between the potential range 1.5 V to 3.95 V and the results are shown in Figure 6. As can be seen from the figure, the voltage-capacity profile is smooth and it is very distinct from $Na_{0.44}MnO_2$ which shows Na insertion/removal through distinct phase transition steps.[22] In $Na_4Mn_4Ti_5O_{18,}$ during the first charge, 1.5 moles of Na is de-intercalated following which nearly 3.2 moles of Na is intercalated on discharge resulting in a capacity of 102 mAh/g or 366 C/g at 0.1C rate. Initial sodium de-intercalation is accompanied by the oxidation of part of $Mn^{3+}$ to $Mn^{4+}$.In subsequent discharge, the reduction proceeds via, $Mn^{4+}$ to $Mn^{3+}$ and further $Mn^{3+}$ to $Mn^{2+}$ at less positive voltages (< 2.7V). Despite the presence of titanium in the phase, it is inactive and does not participate in any redox reactions in the voltage range of interest as evidenced from cyclic voltammetry (see Fig. 5). The lack of clear plateau in the charge – discharge profile and broad peaks with large capacitive currents in cyclic voltammogram (Figure 5) points out the possibility of Na-ion storage in $Na_4Mn_4Ti_5O_{18}$ by capacitive charge storage in addition to intercalation. Electrochemical impedance spectroscopy was employed to analyze the charge storage mechanism in $Na_4Mn_4Ti_5O_{18}$ and the results are presented in Fig. S1. In the linear low frequency region of Nyquist plot, the slope gradually changes from 45 ° to 90° with decrease of ac frequency, indicating that the Na-intercalation in $Na_4Mn_4Ti_5O_{18}$ is not controlled by the diffusion process but through pseudocapacitive processes. [23]

Cyclic voltammograms at varying scan rates (Fig. 7) were recorded to analyze the role of diffusion controlled intercalation process and non-diffusion controlled capacitance process towards the observed total current. According to power law, the current response of a CV is related to scan rate as $i = a\nu^b$, where the exponential factor ‘b’ indicates the charge storage mechanism (b=0.5 for intercalation and b=1 for capacitance).[10,11,24] The slope ‘b’ is obtained from the linear fit of log $i$ vs. log $v$ (Supporting information S2a). The plot of slope ‘b’ as a function of voltage is shown in supporting information S2b. The value of slope ‘b’ varies between 0.5 and 1.0 at most voltages indicating capacitive charge storage in addition to intercalation. It is observed that the diffusion controlled intercalation process dominates at peak potentials and non-diffusion controlled capacitive currents were controlling at other potentials. These results point out that $Na_4Mn_4Ti_5O_{18}$ is a hybrid electrode material possessing both intercalative and capacitive charge storage mechanisms. To ascertain the contribution from intercalation and capacitive processes towards total stored charge, linear fit of $i/(\text{scan rate})^{1/2}$ versus $(\text{scan rate})^{1/2}$ was plotted wherein the slope corresponds to capacitance and the intercept corresponds to intercalation.[11,24] The results indicate that at very low scan rates (<0.05 mV/s), the contribution from intercalation predominates over capacitance towards total stored charge. However at all higher rates, capacitive contribution dominates over intercalation. Charge – discharge curves at fast cycling rates exhibit non triangular type typical of hybrid storage involving intercalation and capacitive charge storage shown in supporting information S3.

Anticipating higher discharge capacity we attempted to extend the cathodic cutoff potential beyond 3.95 V. Irrespective of higher cut off voltage, the discharge capacity stabilized to ~90 mAh/g during initial few cycles. Data and the discussion are presented in Figure S4 in Electronic supporting information. This was further substantiated by impedance spectroscopy (Electronic Supporting information S5) which confirmed electrolyte degradation and increase in SEI resistance. Therefore the upper voltage was limited to 3.95 V in all charging – discharging experiments. Figure 6(b) shows the discharge capacity and the columbic efficiency of $Na_4Mn_4Ti_5O_{18}$ over 50 cycles. Fairly high capacity retention of 90% with quantitative columbic efficiency is observed at the end of 50 cycles.

Rate capability of the electrode materials is derived by cycling at various rates. Figure 8 shows the results of rate capability of $Na_4Mn_4Ti_5O_{18.}$ The compound delivers discharge capacity values of 102, 86, 75 and 60 mAh/g at 0.1C, 0.2C, 0.5C and 1C, respectively. The rate limiting performance of bulk micron sized particles synthesized by solid state necessitates the synthesis of nano material of $Na_4Mn_4Ti_5O_{18}$ which is being presently investigated for the future work.

### Suitability of $Na_4Mn_4Ti_5O_{18}$ for aqueous Na-ion storage applications

Air and moisture stability studies of sodium cathode materials are essential for two reasons, firstly, several of the sodium electrode materials reported are air and moisture sensitive[25] which affect their electrochemical behavior and limit their application. With this perspective, we carried out air and moisture stability test for $Na_4Mn_4Ti_5O_{18.}$ The sample which was exposed to air for 15 days did not show any change in its structure or its electrochemical cycling. In another experiment, the compound was stirred with excess water for at least 48 hours. Then it was allowed to settle resulting in clear supernatant water and settled powder. The supernatant was analyzed for sodium content and the residual powder was dried overnight in oven at 80 °C. The residual powder was subjected to subsequent characterization including X-ray diffraction, Thermogravimetric analysis, surface morphological studies and electrochemical experiments.

Figure 9 compares the X-ray diffraction pattern of as prepared $Na_4Mn_4Ti_5O_{18}$ and after water treatment for 48 hours. It is evident from the figure that there is no perceptible change in the structure due to water treatment. PXRD Rietveld analysis indicated minor decrease in ‘a’ and ‘b’ parameters while ‘c’ parameter show negligible change. The refined lattice parameters for water treated samples are a= 9.2390(4), b=26.4449(4) and c= 2.8912(5). Refinement of different Na site occupancies indicated the Na removal occur at Na3 and Na2 sites, while Na1 sites being unaltered. Kim *et al*. provided possible explanation for changes in lattice parameter and preferential removal of Na from certain sites for isostructural $Na_{0.44}MnO_2$.[26] The exact sodium stoichiometry in the sample after water treatment was determined using AAS. From the analysis, the composition was found to be $Na_{2.9}Mn_4Ti_5O_{18}$ which agrees with the value obtained by Rietveld refinement and also EDS analysis discussed previously (henceforth the composition of $Na_4Mn_4Ti_5O_{18}$ in aqueous medium is referred to $Na_xMn_4Ti_5O_{18}$).Thermogravimetric analysis of the water washed $Na_xMn_4Ti_5O_{18}$ did not show any weight loss up to 700 °C indicating absence of hydrated water or proton.

Enthused by the above results, we explored the performance of $Na_xMn_4Ti_5O_{18}$ as cathode material for aqueous sodium ion storage using 1 M $Na_2SO_4$ aqueous electrolyte. Figure 10 shows the cyclic voltammogram of $Na_xMn_4Ti_5O_{18}$ in 1 M $Na_2SO_4$ at a scan rate of 0.1 mV/s in the voltage range -0.2 V to 1 V. At voltages below -0.2 V and above 1 V, electrolytic decomposition of water is observed. There exist one pair of oxidation and reduction peaks at 0.37 V / 0.29 V, respectively which are assigned to $Mn^{3+}/Mn^{4+}$ redox couple. Galvanostatic charge discharge experiments were performed in the voltage range 0 V to 0.8 V with three electrode configuration and the results are shown in Fig.11. The first discharge capacity of 36 mAh/g was observed corresponding to reversible insertion of 1.1 moles of sodium onto $Na_xMn_4Ti_5O_{18}$ structure or 0.275 moles of sodium for every mole Mn. It corresponds to a specific capacitance of 144 F/g (115C/g / 0. 8V). The sample exhibited capacity retention of about 70% for over 100 cycles (Fig. 11(b)) in aqueous medium.

## CONCLUSIONS

Framework structured $Na_4Mn_4Ti_5O_{18}$ was prepared by solid state method. It crystallize in *Pbam* orthorhombic space group with lattice parameters a = 9.2493(1), b = 26.4599(4), c = 2.8926(3) (Å). X-ray photoelectron spectroscopy indicated the chemical state of Mn and Ti in the pristine phase to be trivalent and tetravalent, respectively. $Na_4Mn_4Ti_5O_{18}$ delivered a reversible capacity of 102 mAh/g (C/10) between 3.95-1.5 V in organic electrolyte with capacity retention of 90% over 50 cycles. Electrochemical analysis indicated the total stored charge corresponds to cumulative contributions originating from diffusion controlled intercalation and non-diffusion controlled capacitance. At very slow scan rates, intercalation contribution was dominant and at all higher rates capacitance component was larger. In aqueous medium, the sample forms non-stoichiometric sodium phase, $Na_xMn_4Ti_5O_{18}$ (x is 2.8-3.2 mole) and yet retain the framework structure. The non-stoichiometric sodium phase, $Na_xMn_4Ti_5O_{18}$ is investigated for aqueous sodium-ion storage. It exhibited a capacity of about 36 mAh/g (C/10) in the voltage window of 0-0.8 V in 1M $Na_2SO_4$ electrolyte. The study points out the pseudocapacitive Na-ion storage mechanism in the framework $Na_4Mn_4Ti_5O_{18}$ suitable for Na-ion storage in non-aqueous and aqueous electrolytes.

## SUPPORTING INFORMATION

Five figures showing impedance spectroscopy of charged sample, electrochemical analysis of cyclic voltammetry, fast cycling data of $Na_4Mn_4Ti_5O_{18,}$ electrochemical performance at different potentials and corresponding electrochemical impedance spectra are presented.

## AUTHOR INFORMATION

Corresponding Author: Dr. A. S. Prakash (Email: prakash.as@gmail.com). Phone: +91-44-22544560

## ACKNOWLEDGEMENT

The authors thank the Council of Scientific and Industrial Research (CSIR), India for support of this work under the TAPSUN project of CSIR. Dr. M. Jayakumar thanks CSIR for granting CSIR Nehru Postdoctoral Fellowship. Ms. K. Hemalatha thanks CSIR for granting Senior Research Fellowship. The authors thank Central Instrumentation Facility, CECRI, Karaikudi and CSIR Innovation complex facilities, CSIR Madras Complex, Chennai for providing characterization facilities.

## REFERENCES

1 J. M. Tarascon and M. Armand, *Nature* 2001, **414**, 359-367.

2 N. Yabuuchi, M. Kajiyama, J. Iwatate, H. Nishikawa, S. Hitomi, R. Okuyama, T. Usui, Y. Yamada and S. Komaba, *Nature Mat*. 2012, **11**, 512-517.

3 V. Palomares, P. Serras, I. Villaluenga, K.B. Hueso, J. Carretero-Gonzalez and T. Rojo, *Energy Environ. Sci*. 2012, **5**, 5884-5901.

4 S.W. Kim, D.H. Seo, X. Ma, G. Ceder and K. Kang, *Adv. Energy Mater*. 2012, **2**, 710-721.

5 M. D. Slater, D. Kim, E. Lee and C. S Johnson, *Adv. Funct. Mater*. 2013, **23**, 947-958.

6 H. Pan, Y.S. Hu and L. Chen, *Energy Environ. Sci.* 2013, **6**, 2338-2360.

7 S.I. Park, I. Gocheva, S. Okada and J. Yamaki, *J. Electrochem. Soc.* 2011, **58**, 1-4.

8 (a) Z. Li, D. Young, K. Xiang, W.C. Carter and Y.M. Chiang, *Adv. Energy Mater*. 2012, **3**, 290 - 294; (b) J.F. Whitacre, A. Tevar, S. Sharma, *Electrochem. Comm.*, 2010, **12**, 463-466; (c) G. Pang, P. Nie, C. Yuan, L. Shen, X. Zhang, J. Zhu and B. Ding, *Energy Tech.* 2014, **2,** 705-712

9 V. Augustyn, P. Simon and B. Dunn, *Energy Environ. Sci*. 2014, **7**, 1597-1614.

10 T. Brezesinski, J.Wang, S. H. Tolbert and B. Dunn, *Nat. Mat*. 2010, **9**, 146-151.

11 M. Sathiya, A. S. Prakash, K. Ramesha, J-M. Tarascon and A. K. Shukla, *J. Am. Chem. Soc. 2011*, **133**, 16291–16299

12 M. Sathiya, A. M. Abakumov, D. Foix, G. Rousse, K. Ramesha, M. Saubanère, M. L. Doublet, H. Vezin, C. P. Laisa, A. S. Prakash, D. Gonbeau, G. VanTendeloo and J-M. Tarascon, *Nature Materials* 2015, **14**, 230–238

13 B. Senthilkumar, K. V. Sankar, L. Vasylechko, Y-S.Lee and R. K. Selvan, *RSC Adv.*, 2014, **4,** 53192-53200.

14 S. Guo, H. Yu, D. Liu, W. Tian, X. Liu, N. Hanada, M. Ishida and H. Zhou, *Chem. Commun.*,2014, **50**, 7998-8001

15 W. G. Mumme, *Acta Cryst.*, 1968, **24**, 1114-1120.

16 H. M. Rietveld, *J. Appl. Crystallogr*. 1969, **2**, 65-71.

17 J. Rodriguez-Carvajal, *Physica B* 1993, **192**, 55-69.

18 J. Li, S. Tang, L. Lu and H. C. Zeng, *J. Am. Chem. Soc*. 2007, **129**, 9401-9409.

19 M. C. Biesinger, B.P. Payne, A.P. Grosvenor, L.W.M. Lau, A. R. Gerson and R. Smart, *Appl. Surf. Sci*. 2011, **257**, 2717-2730.

20 R. Dedryve`re, D. Foix, S. Franger, S. Patoux, L. Daniel and D. Gonbeau, *J. Phys. Chem. C* 2010, **114**, 10999-11008.

21 Y. Xu, E. M. Lotfbad, H. Wang, B. Farbod, Z. Xu, A. Kohandehghan and D. Mitlin, *Chem. Comm.* 2013, **49**, 8973-8975.

22 F. Sauvage, L. Laffont, J.-M. Tarascon and E. Baudrin, *Inorg. Chem.*, 2007, **46**, 3289-3294

23 B. E. Conway, *Electrochemical Supercapacitors: Scientific Fundamentals and Technological Applications*, Kluwer Academic/Plenum Publishers, **1999**.

24 K. Hemalatha, A. S. Prakash, Guruprakash K and M. Jayakumar, *J. Mat Chem A*, 2014, **2**, 1757-1766

25 M. Sathiya, K. Hemalatha, K. Ramesha, J. M. Tarascon and A. S. Prakash, *Chem. Mater.* 2012, **24**, 1846-1853.

26 H. Kim, D.J. Kim, D.H. Seo, M. S. Yeom, K. Kang, D.K. Kim and Y. Jung, *Chem. Mater.* 2012, **24**, 1205-1211

**Table 1. Refined crystallographic parameters obtained from XRD Rietveld fit of pristine $Na_4Mn_4Ti_5O_{18}$ using Fullprof Suite**

| Site | Np | Wyckoff position | x | y | z |
|---|---|---|---|---|---|
| Ti1 | 2 | 2c | 0.0000 | 0.5000 | 0.0000 |
| Ti2 | 4 | 4h | 0.3647 | 0.3050 | 0.5000 |
| Ti3 | 4 | 4g | 0.0111 | 0.1063 | 0.0000 |
| Mn1 | 4 | 4g | 0.0325 | 0.3086 | 0.0000 |
| Mn2 | 4 | 4h | 0.3603 | 0.0885 | 0.5000 |
| Na1 | 4 | 4g | 0.2129 | 0.2096 | 0.0000 |
| Na2 | 4 | 4h | 0.2061 | 0.4186 | 0.5000 |
| Na3 | 4 | 4g | 0.1214 | 0.0014 | 0.0000 |
| O1 | 4 | 4h | 0.3512 | 0.0002 | 0.5000 |
| O2 | 4 | 4g | 0.2265 | 0.0990 | 0.0000 |
| O3 | 4 | 4h | 0.0493 | 0.1588 | 0.5000 |
| O4 | 4 | 4h | 0.4228 | 0.1658 | 0.5000 |
| O5 | 4 | 4h | 0.1459 | 0.2883 | 0.5000 |
| O6 | 4 | 4g | 0.4188 | 0.2627 | 0.0000 |
| O7 | 4 | 4g | 0.3274 | 0.3512 | 0.0000 |
| O8 | 4 | 4g | 0.5167 | 0.0748 | 0.0000 |
| O9 | 4 | 4h | 0.4536 | 0.4402 | 0.5000 |

Lattice parameters : a(Å) = 9.2493(1), b(Å) = 26.4599(4), c(Å) = 2.8926(3), Space group : *Pbam*(55), $\chi^2 = 3.52$.

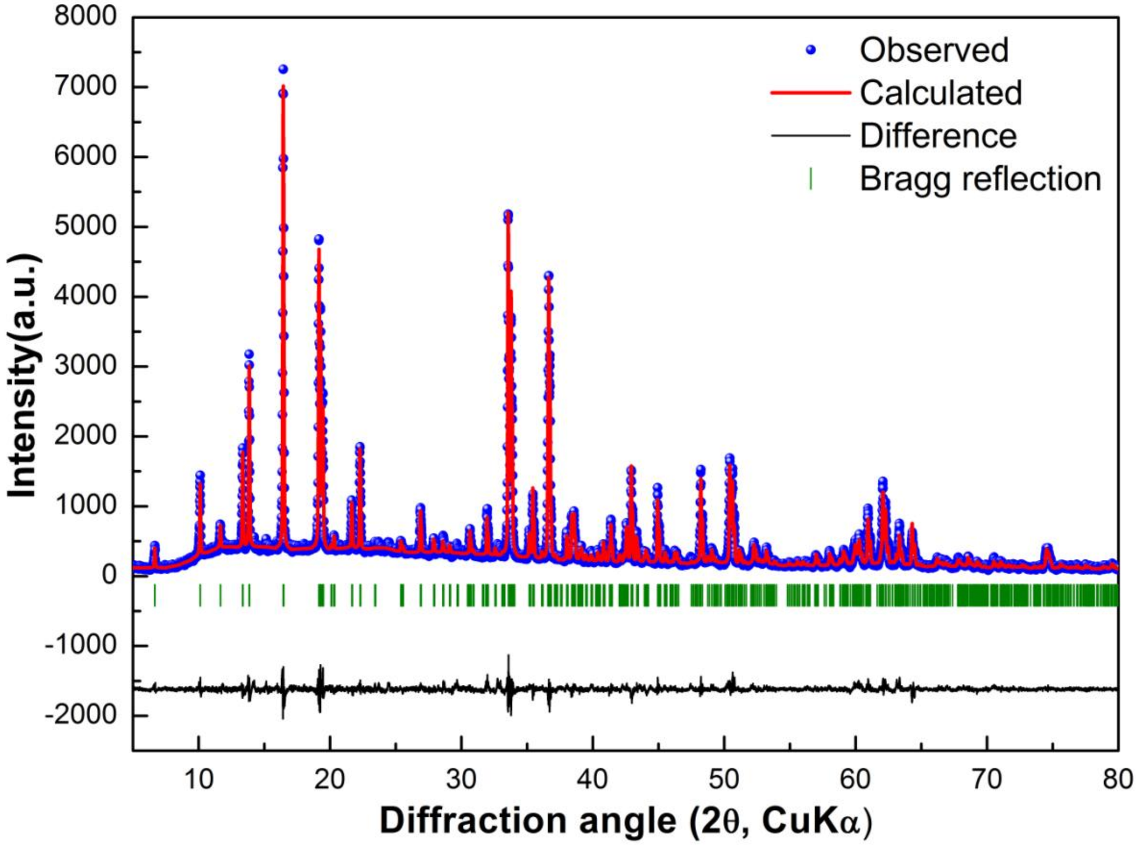

**Figure 1. Powder XRD and Rietveld refinement fit of $Na_4Mn_4Ti_5O_{18}$.** The pattern was refined with *pbam* model system using Fullprof suite program. The experimental pattern, Rietveld fit and the Bragg positions are shown in blue points, red lines and green vertical ticks, respectively. The black line is the difference between the observed and calculated patterns.

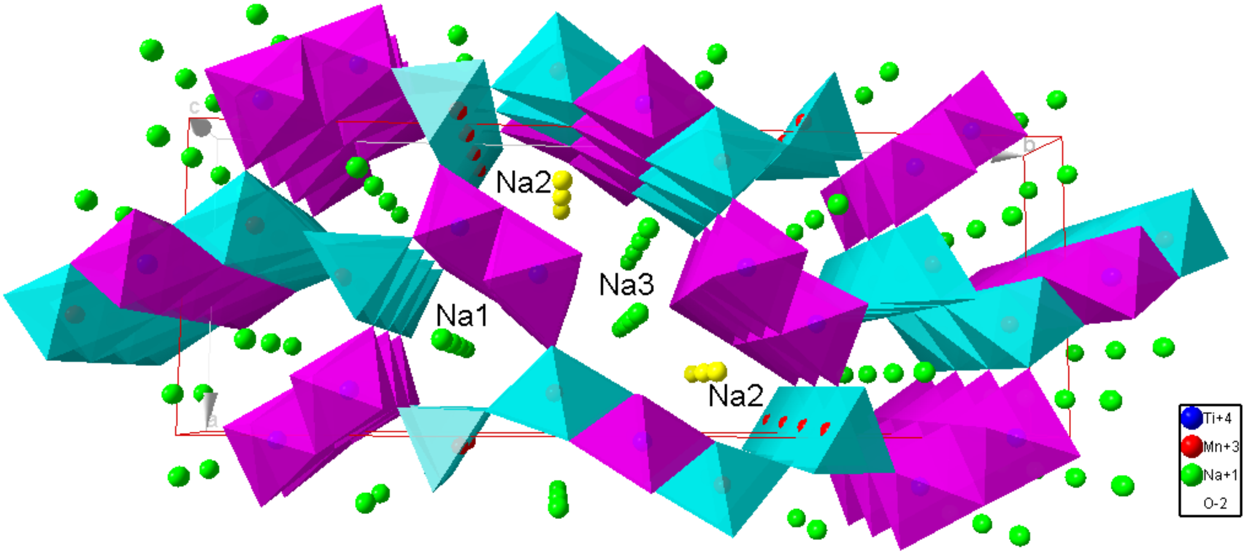

**Figure 2. Structure of $Na_4Mn_4Ti_5O_{18}$ viewing along c-axis.** The structure contains two types of tunnels - a large flat S shaped tunnel containing partially filled sites for four Na-ions and another relatively smaller hexagonal tunnel with centrally located single Na-ion. $Ti^{4+}$ (blue spheres) in octahedral coordination is shown in magenta fill and $Mn^{3+}$ (red spheres) coordination is shown in cyan fill. While one $Mn^{3+}$ exists in octahedral coordination and another in rectangular pyramid coordination. Na-ion occupies two positions, 4g (green spheres) and 4h (yellow spheres) in the centre S-shaped tunnel.

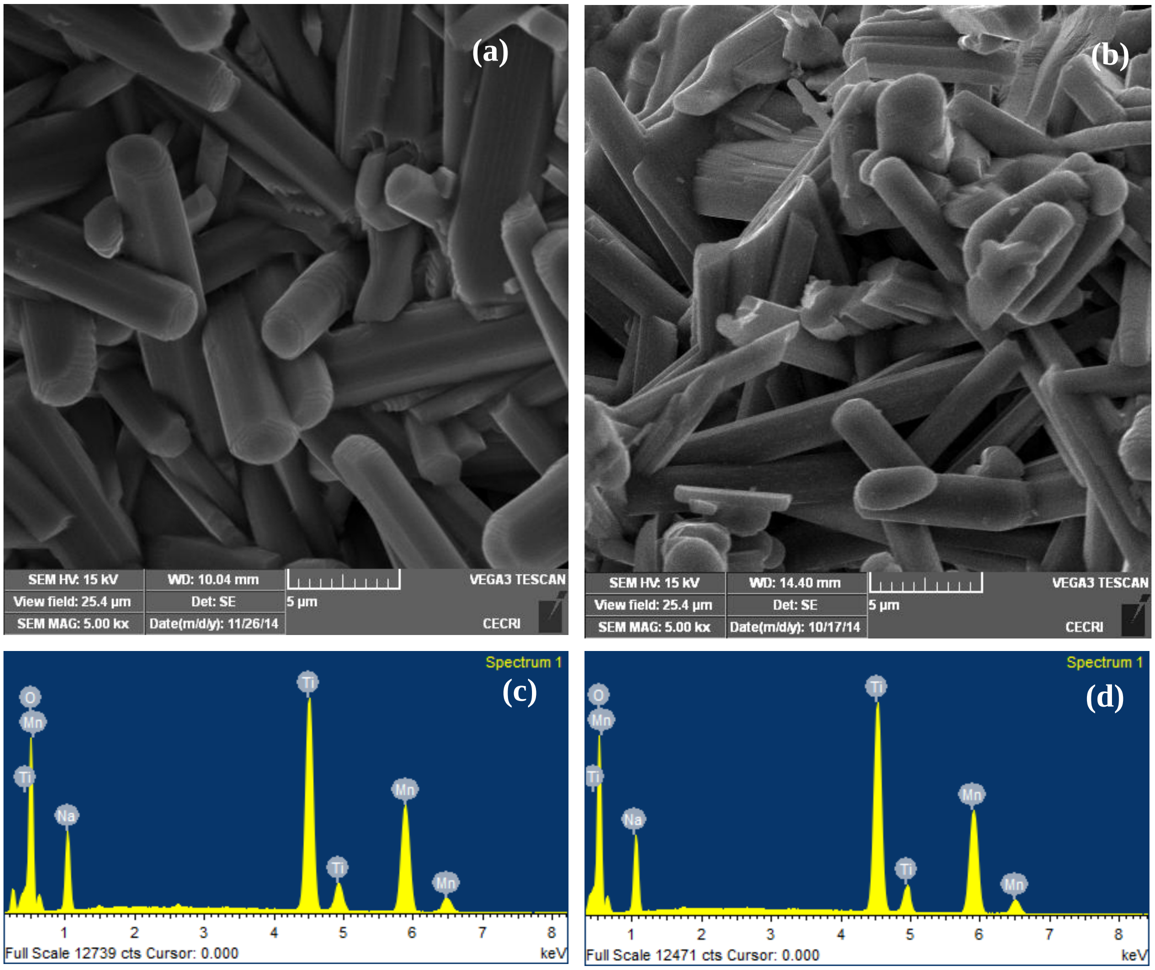

| Element | Atomic percentage | |
|---|---|---|
| | Pristine | Post water wash |
| Na | 12.2 | 9.6 |
| Ti | 15.8 | 16.1 |
| Mn | 12.6 | 13.0 |
| O | 59.4 | 61.3 |
| Total | 100.00 | 100.00 |

**Figure 3. Surface morphology and elemental composition of $Na_4Mn_4Ti_5O_{18}$.** SEM images of (a) pristine $Na_4Mn_4Ti_5O_{18}$ (b) after stirred with water for 48 h followed by filtration and oven drying at 80°C for 10 h. EDS pattern of (c) pristine $Na_4Mn_4Ti_5O_{18}$ and (d) after water wash. Corresponding elemental composition are shown below the respective spectrum.

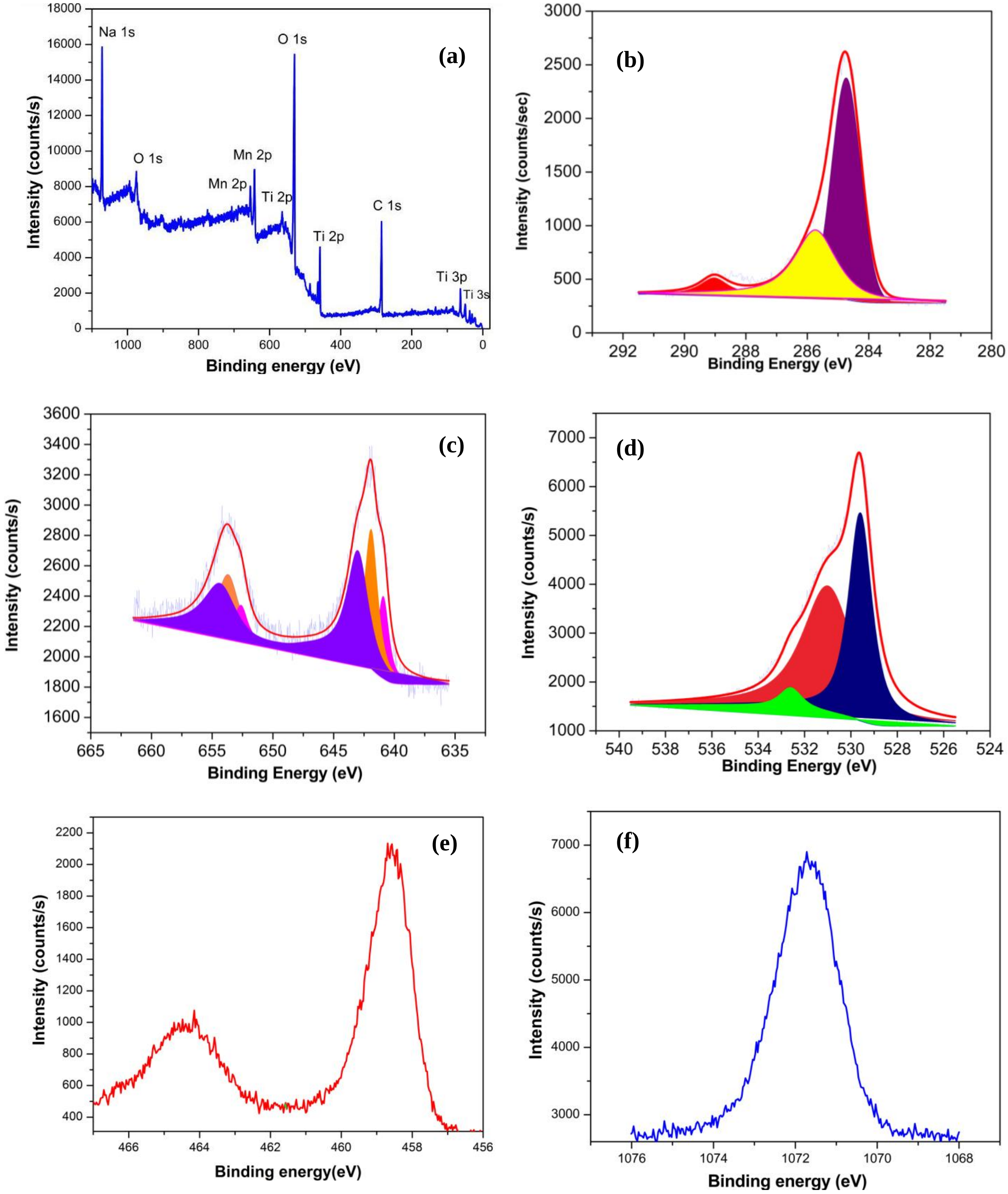

**Figure 4(a): X-ray photoelectron spectrum of pristine $Na_4Mn_4Ti_5O_{18}$.** (a) Survey spectrum indicating the presence of C (1s), Mn (2p), O (1s), Ti (2p) and Na (1s) originating from the sample. (b) Deconvoluted C (1s) region showing adventitious, defective and carboxyl carbons. (c) Deconvoluted Mn ($2p_{3/2,\ 1/2}$) region to show $Mn^{3+}$ in different environments. (d) Deconvoluted O (1s) region indicating lattice oxygen with coordination deficiency and surface adsorbed oxygen. (e) The Ti (2p) binding energy region showing spin orbit splitting of $2p_{3/2}$ and $2p_{1/2}$. (f) Characteristic binding energy of Na 1s.

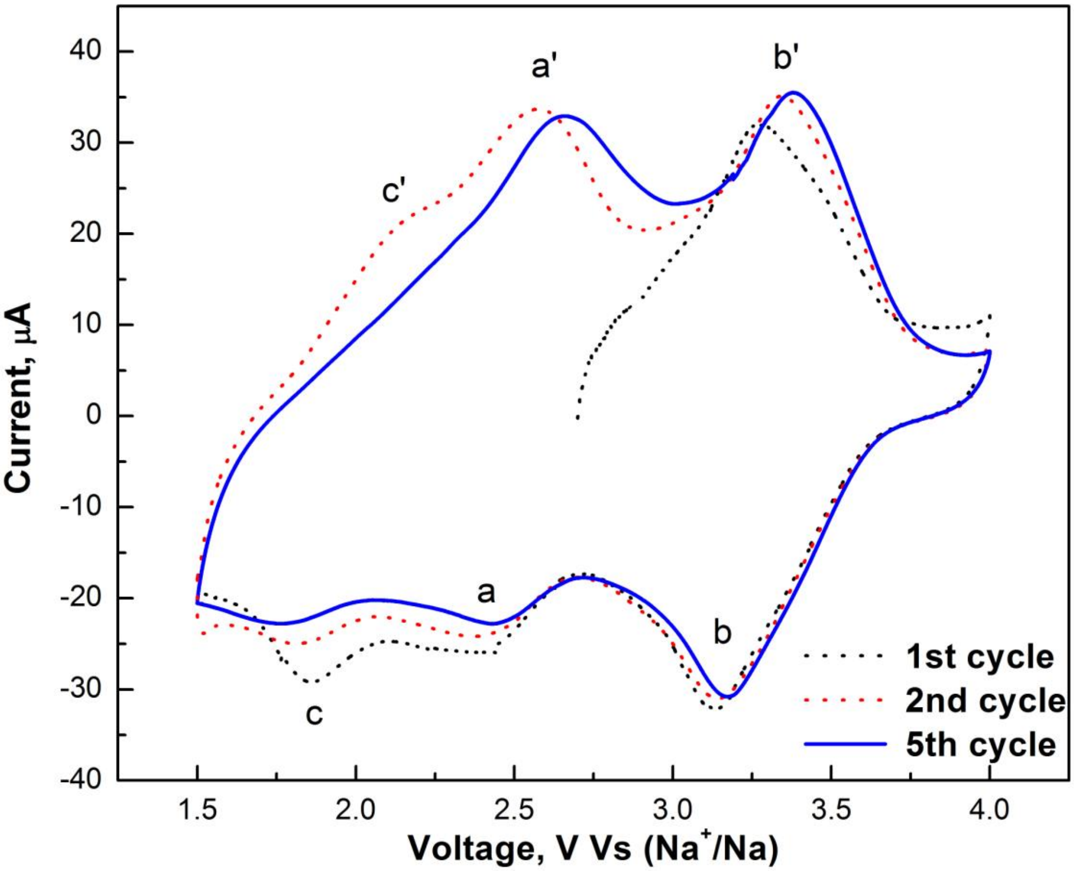

**Figure 5. Cyclic voltammetry of $Na_4Mn_4Ti_5O_{18}$ Vs. Na in 1 M $NaPF_6$ / EC-DMC (1:1) electrolyte at a scan rate of 0.1 mV/s.** The first charging cycle shows only one oxidation peak corresponding to $Mn^{3+}/Mn^{4+}$ couple ( indicated as b') while two peaks are observed during the voltage reversal pertaining to $Mn^{4+}/Mn^{3+}$ (indicated as b) and $Mn^{3+}/Mn^{2+}$(indicated as a) reduction reactions. Minor peaks (noted as c/c') are due to structural rearrangement of the lattice in the initial cycles.

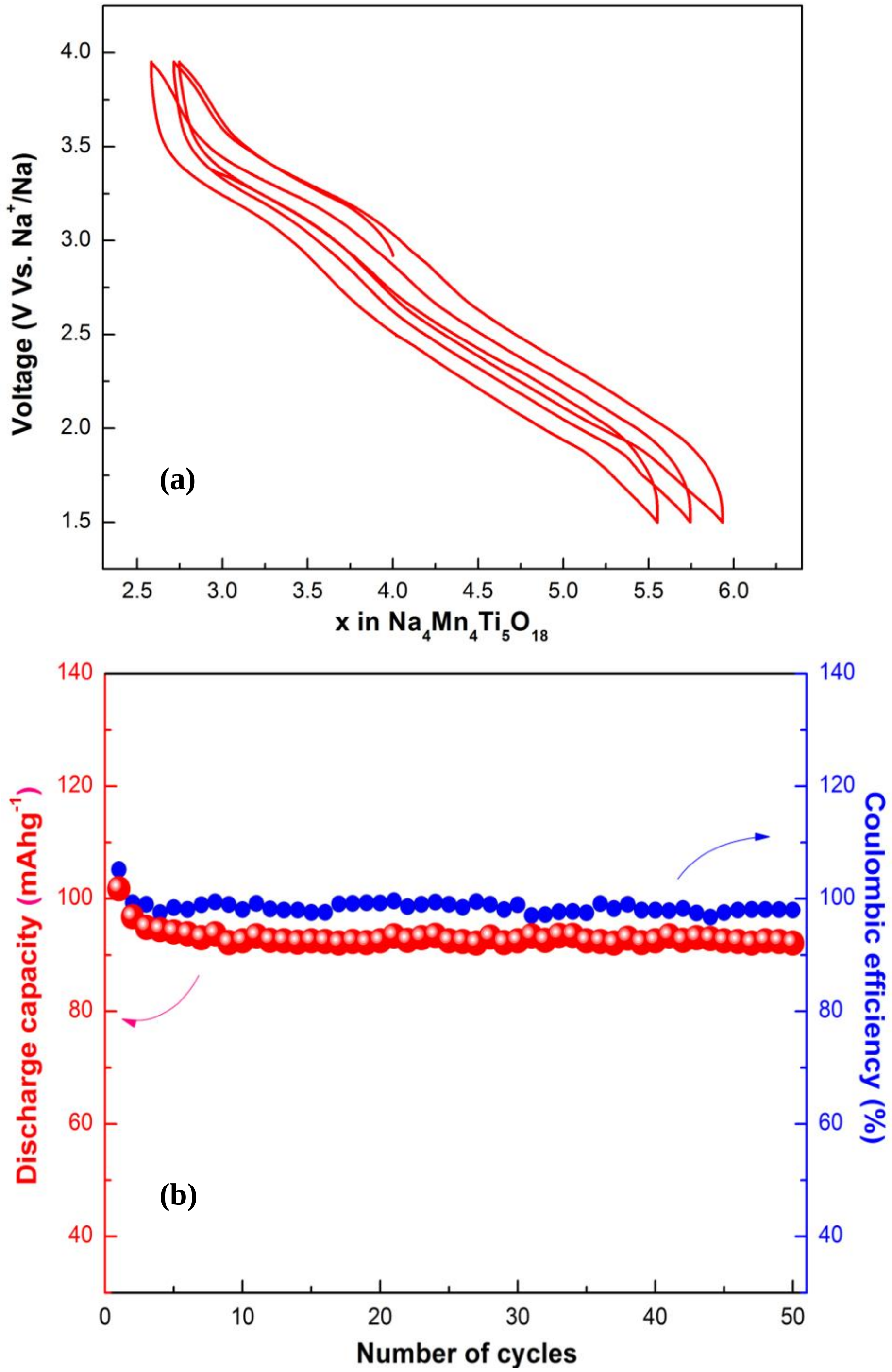

**Figure 6. Electrochemical performance of $Na_4Mn_4Ti_5O_{18}$ as cathode material for sodium ion storage.** (a) Voltage-composition plot obtained by galvanostatic charge-discharge cycling of $Na_4Mn_4Ti_5O_{18}$ Vs Na in the voltage range 1.5 V to 3.95 V at C/10 rate. Cycling was done at room temperature using 1 M $NaPF_6$ : EC-DMC (1:1) electrolyte; (b) Discharge capacity (Red spheres) and columbic efficiency (blue spheres) versus cycle number.

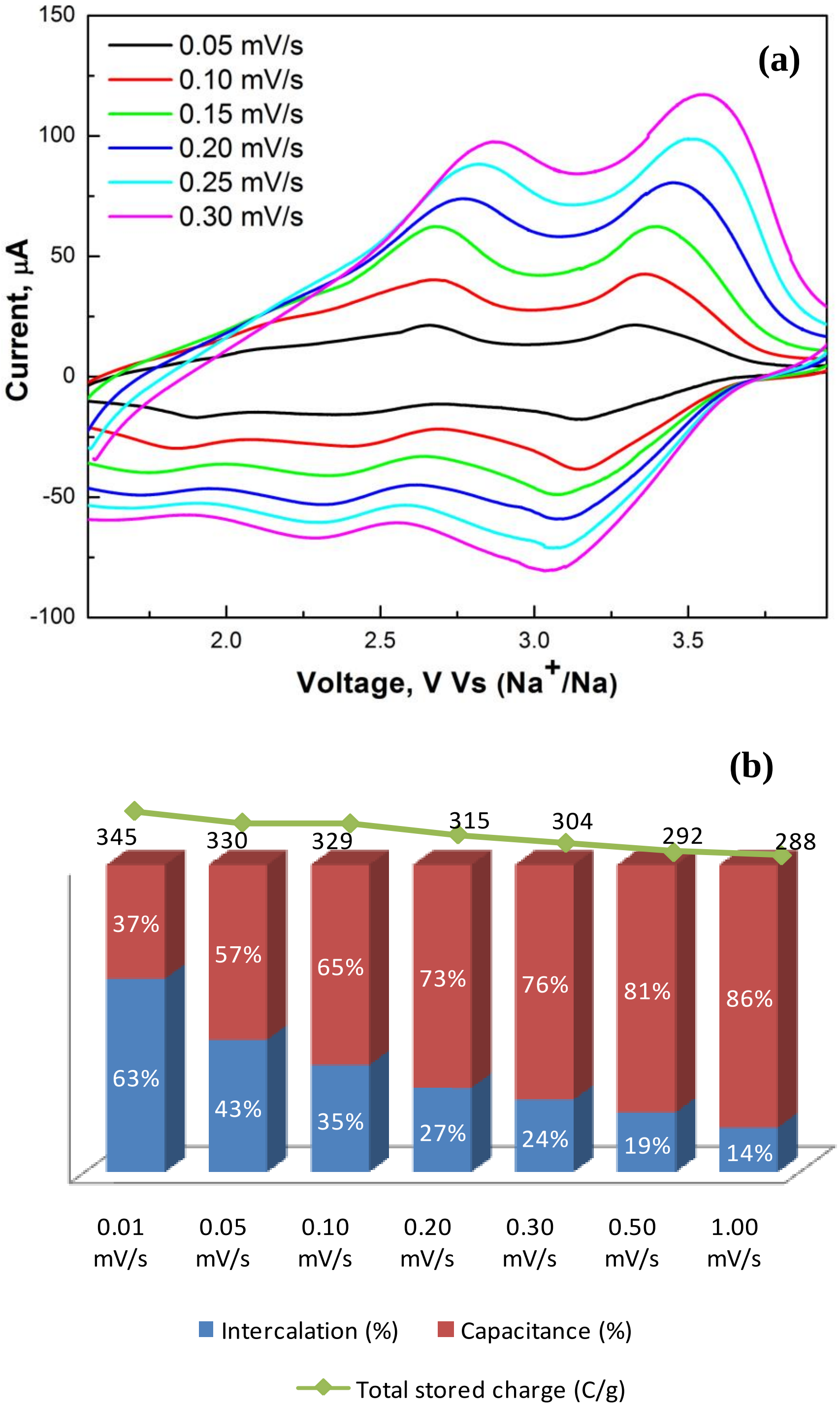

**Figure 7. Electrochemical analysis of charge storage in $Na_4Mn_4Ti_5O_{18}$ by cyclic voltammetry** (a) Cyclic voltammograms of $Na_4Mn_4Ti_5O_{18}$ at different scan rates. (b) Contributions from intercalation and capacitance towards total stored charge in $Na_4Mn_4Ti_5O_{18}$. All cyclic voltammetry experiments were performed with IR compensation.

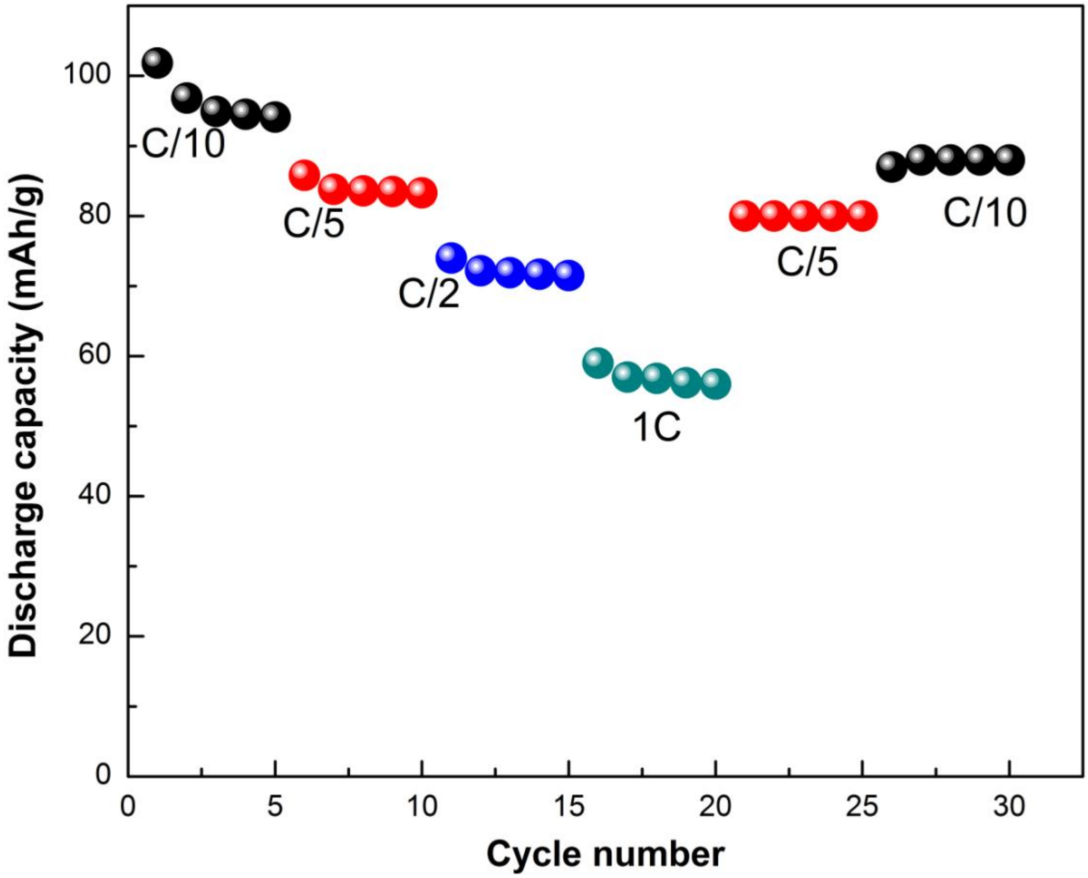

**Figure 8. Rate capability studies on $Na_4Mn_4Ti_5O_{18}$ Vs. Na cell.** The cell was subjected to charge – discharge cycling at C/10, C/5, C/2 and 1C rates. C/10 rate refers to removal/insertion of one mole of Na per formula unit in 10 hours and corresponds to a current density of 12.8 mA/g

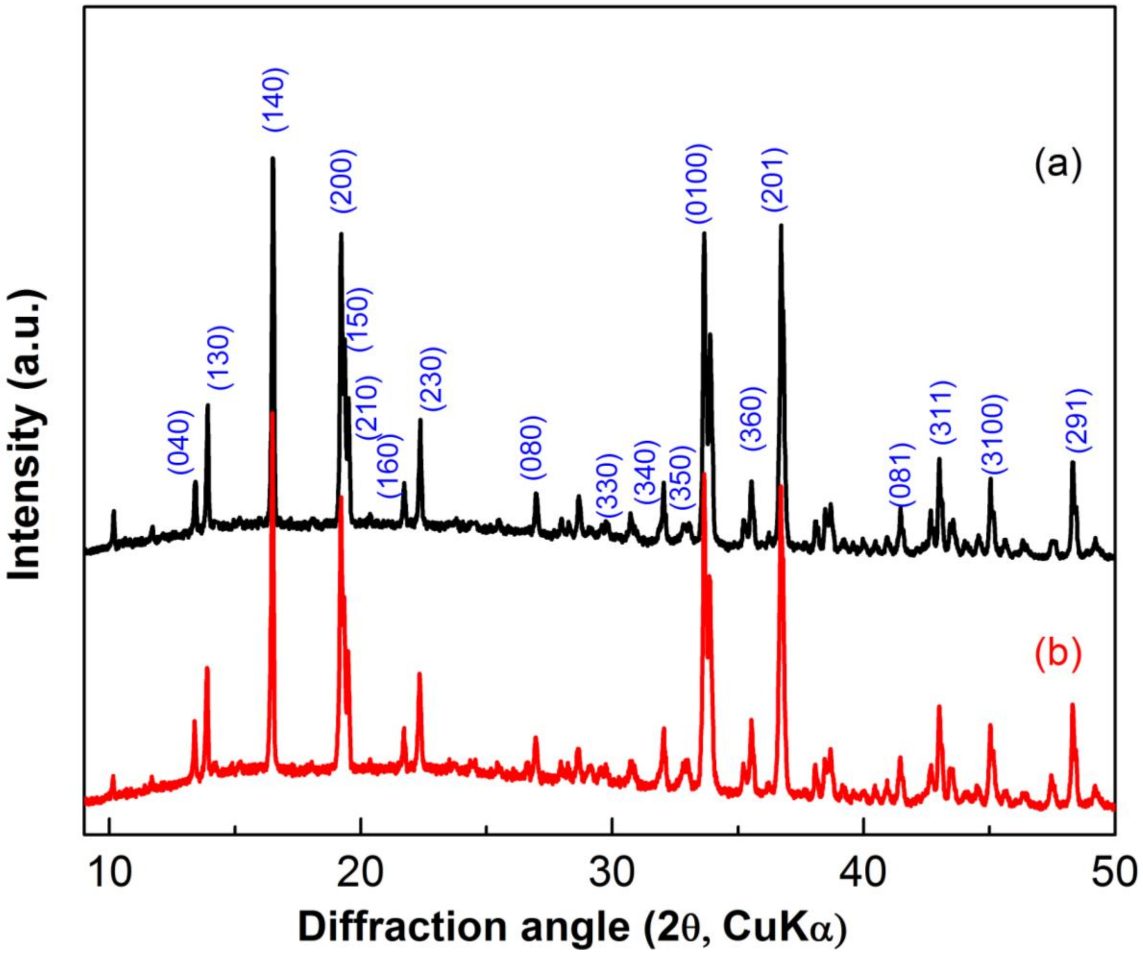

**Figure 9. Powder X-ray diffraction data** of (a) pristine $Na_4Mn_4Ti_5O_{18}$ and (b) samples stirred in water for 48 hours and dried in oven.

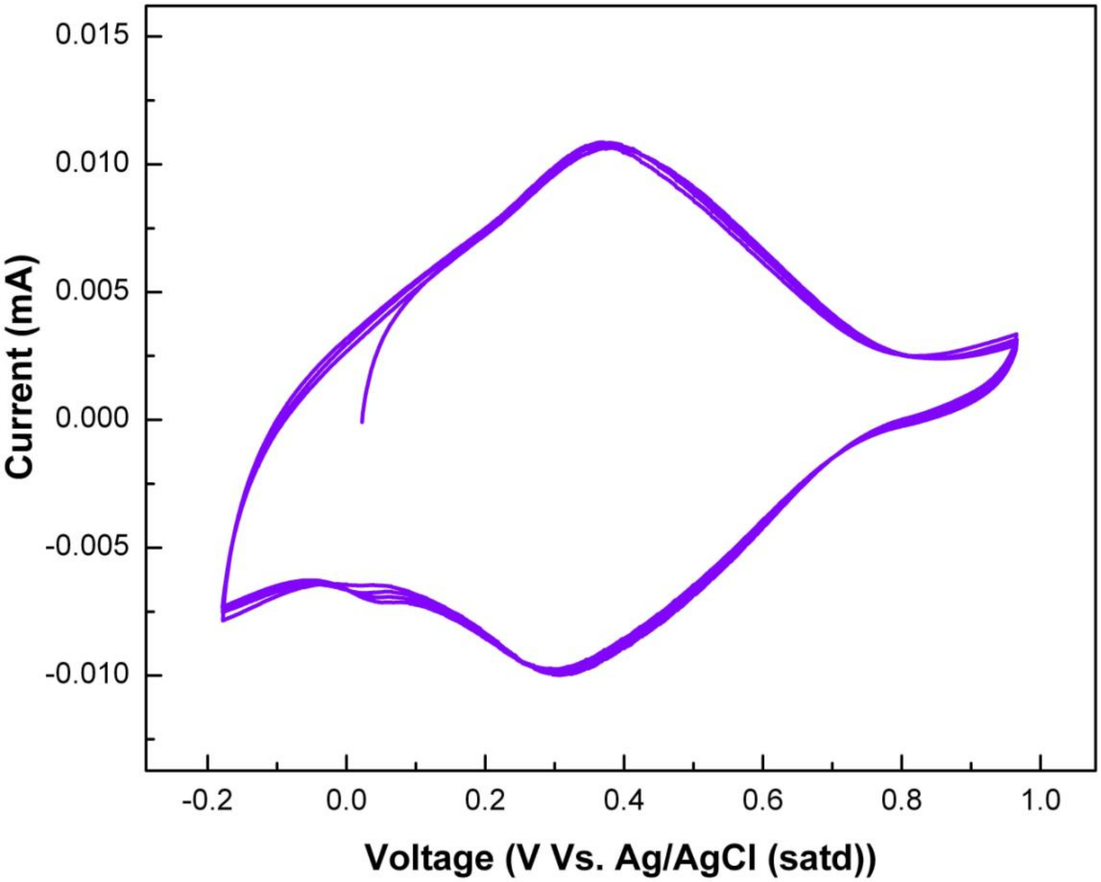

**Figure 10. Cyclic voltammetry of $Na_4Mn_4Ti_5O_{18}$ recorded in 1 M $Na_2SO_4$** using platinum counter and Ag/AgCl (satd) reference electrode at a scan rate of 0.1 mV/s. The working electrode was $Na_4Mn_4Ti_5O_{18}$ coated glassy carbon.

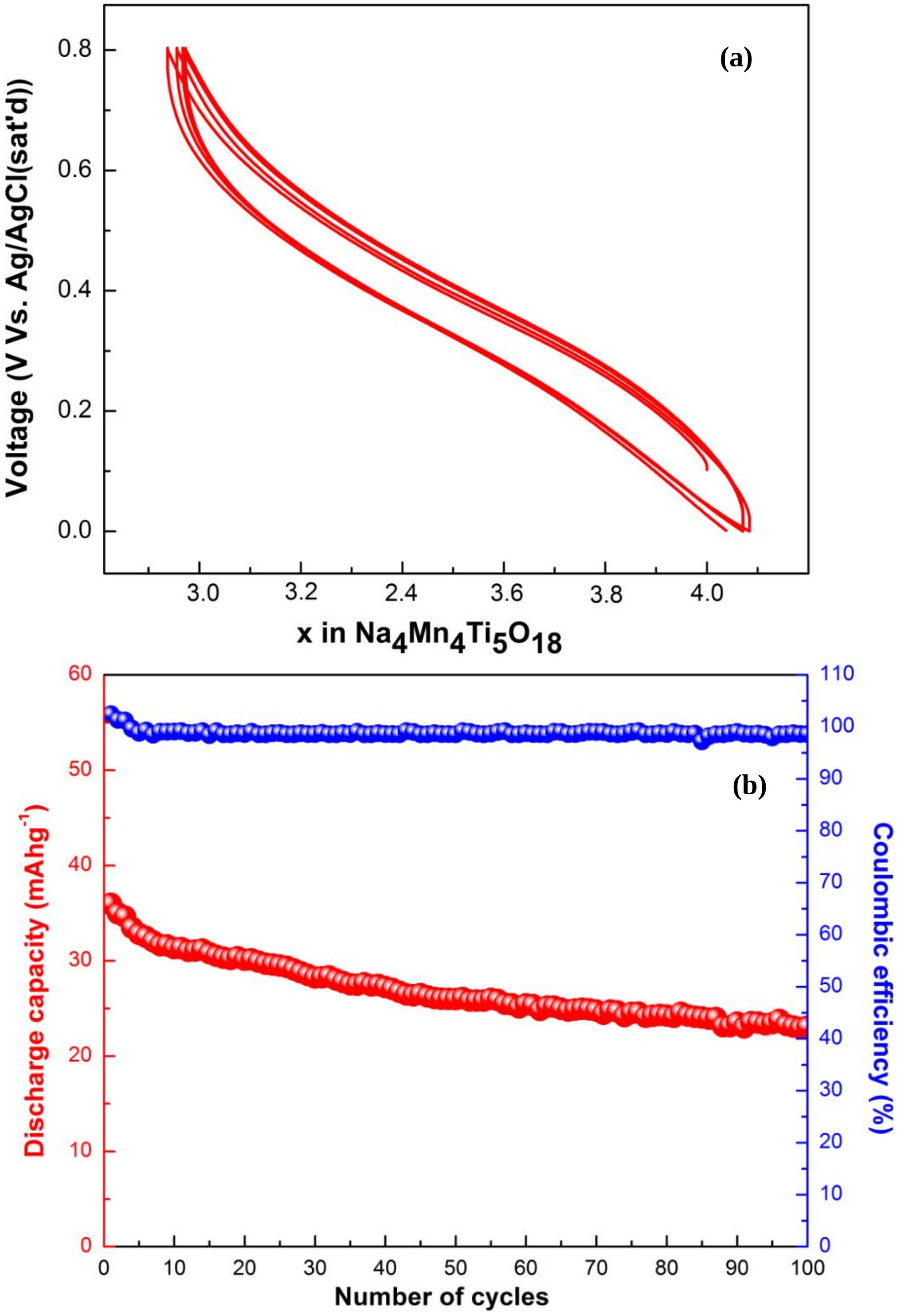

**Figure 11. Performance of $Na_4Mn_4Ti_5O_{18}$ in aqueous electrolytes** (a) Voltage-composition plot obtained by galvanostatic charge-discharge cycling of $Na_4Mn_4Ti_5O_{18}$ against platinum counter electrode in 1 M $Na_2SO_4$ between 0 to 0.8 V (Vs Ag/AgCl(saturated)) (b) Capacity retention of $Na_4Mn_4Ti_5O_{18}$ coated on glassy carbon electrode in aqueous electrolyte.